Computerized Medical Imaging and Graphics 106 (2023) 102203

Contents lists available at ScienceDirect

Computerized Medical Imaging and Graphics

journal homepage: www.elsevier.com/locate/compmedimag

# Image-based estimation of the left ventricular cavity volume using deep learning and Gaussian process with cardio-mechanical applications

Arash Rabbani [a,b,*], Hao Gao [a], Alan Lazarus [a], David Dalton [a], Yuzhang Ge [a], Kenneth Mangion [c], Colin Berry [c], Dirk Husmeier [a]

[a] School of Mathematics & Statistics, University of Glasgow, Glasgow G12 8QQ, United Kingdom
[b] School of Computing, University of Leeds, Leeds LS2 9JT, United Kingdom
[c] School of Cardiovascular & Metabolic Health, University of Glasgow, Glasgow G12 8QQ, United Kingdom

ARTICLE INFO

Dataset link: https://github.com/ArashRabbani/VentricleVolume

*Keywords:*
Cardiac magnetic resonance imaging
Deep learning
Gaussian process

ABSTRACT

In this investigation, an image-based method has been developed to estimate the volume of the left ventricular cavity using cardiac magnetic resonance (CMR) imaging data. Deep learning and Gaussian processes have been applied to bring the estimations closer to the cavity volumes manually extracted. CMR data from 339 patients and healthy volunteers have been used to train a stepwise regression model that can estimate the volume of the left ventricular cavity at the beginning and end of diastole. We have decreased the root mean square error (RMSE) of cavity volume estimation approximately from 13 to 8 ml compared to the common practice in the literature. Considering the RMSE of manual measurements is approximately 4 ml on the same dataset, 8 ml of error is notable for a fully automated estimation method, which needs no supervision or user-hours once it has been trained. Additionally, to demonstrate a clinically relevant application of automatically estimated volumes, we inferred the passive material properties of the myocardium given the volume estimates using a well-validated cardiac model. These material properties can be further used for patient treatment planning and diagnosis.

## 1. Introduction

In this section, after describing the motivations for the present study, the limitations of the preexisting approaches are discussed and our contribution to the literature is provided. In addition, a brief background on related cardio-mechanical applications is presented to help emphasizing the clinical implications of the proposed method.

### 1.1. Motivation

Cardiovascular disease (CVD) is one of the leading causes of death in the United States and many parts of the world, and its prevalence is predicted to increase in the years to come (Heidenreich et al., 2011; Stevens et al., 2016). The Journal of the American College of Cardiology has reported that global CVD cases have almost doubled between 1990 and 2019, increasing from 271 million to 523 million (Roth et al., 2020). These figures highlight the significant role of quantitative research studies and patient-specific treatments of CVDs in responding effectively to future challenges. In the past decade, cardiac magnetic resonance (CMR) imaging has proven to be a critical tool in the diagnosis of complex cardiovascular diseases, from myocardial infarction to hypertrophy and injury (Bucciarelli-Ducci et al., 2020; Mangold et al., 2013). CMR imaging is considered one of the most accurate approaches to measuring the ejection fraction, ventricular mass, myocardial volume, and stroke volumes (Khened et al., 2019) which are critical for the detection of certain CVDs (Bernard et al., 2018). However, O'Dell (2019) reported that when using common geometric assumptions with a limited number of short-axis slices, the expected uncertainty of the measurement of the ejection fraction can reach 49%. O'Dell (2019) further added that by including six or more short-axis slices, the composite midpoint integration method, which is common practice, can achieve an error in the ejection fraction of less than 3% and a volume error in the left ventricular (LV) cavity of approximately 10% compared to manually segmented slices. However, taking into account the time-consuming process of manual segmentation of CMR images and the limited accuracy of conventional methods for estimating the LV cavity volume, an automated volume estimation approach is favorable to minimize the required man-hours and maintain a reasonable level of accuracy. As one of the mainstream automated methods to tackle this problem, deep machine learning will be discussed in more detail.

* Corresponding author at: School of Computing, University of Leeds, Leeds LS2 9JT, United Kingdom.
*E-mail address:* a.rabbani@leeds.ac.uk (A. Rabbani).

https://doi.org/10.1016/j.compmedimag.2023.102203
Received 2 September 2022; Received in revised form 26 November 2022; Accepted 17 February 2023
Available online 24 February 2023

### 1.2. Application of deep learning and limitations

In recent years, deep learning has emerged as the leading automated approach for image-based characterization of the heart (Chen et al., 2020; Hernandez et al., 2021; Dalton et al., 2021), having achieved state-of-the-art results in cardiac image segmentation (Bernard et al., 2018; Khened et al., 2018; Isensee et al., 2017) and cardiac disease diagnosis (Isensee et al., 2017; Wolterink et al., 2017). Automated deep learning analysis of the left ventricle specifically has been of great interest (van Hamersvelt et al., 2019; Liu et al., 2021), in particular for extracting its volume (Isensee et al., 2017; Khened et al., 2019). One problem, however, with automated deep learning approaches is that they are not guaranteed to produce results that respect the known anatomical features of the heart. For segmentation tasks, for example, any artifacts in the CMR images can be passed on by the automated method to the segmentation output, potentially yielding non-physiological results, such as holes in the myocardium.

Knowing the mentioned limitation, we review the conventional automated procedure for estimating the volume of LV. For this purpose, a trained deep learning model segments the LV cavity in several short-axis CMR images. Knowing the vertical spacing of the slices and the spatial resolution of the images, an approximate 3D voxelized shape of the LV can then be reconstructed. Counting the number of voxels within the cavity and multiplying it by the spatial resolution gives the approximate cavity volume, as demonstrated by Isensee et al. (2017) and Khened et al. (2019). The voxelized shape of the left ventricle reconstructed in this manner has very rough edges, which do not respect the smoothness of the heart wall. Several approaches have been proposed to incorporate prior knowledge of cardiac anatomy in image segmentation and geometry reconstruction tasks. This includes the use of shape priors (Duan et al., 2019; Oktay et al., 2017), constraining the reconstructed geometry to lie on a linear PCA subspace (Romaszko et al., 2021), as well as warping methods based on a low-dimensional embedding of the LV anatomy found with a constrained variational autoencoder (Painchaud et al., 2020). To date, however, incorporating prior anatomical knowledge into volume estimation tasks has received less attention.

### 1.3. Contribution to the literature

The present work expands the literature on automatic LV cavity volume extraction from CMR scans by taking into account the continuity and smoothness of the heart wall in both space and time. Our approach is based on flexible Gaussian process regression, which, as we will demonstrate, achieves significantly improved accuracy. An important application of the estimation of the volume of the LV cavity is in the detection of cardiovascular diseases (Bernard et al., 2018). Furthermore, cardio-mechanical models can use these volume estimations to infer the mechanical properties of the myocardium non-invasively (Hadjicharalambous et al., 2015; Gao et al., 2017b). Considering the importance of cardio-mechanical models as a complementary step to the presented volume estimation method, a brief background is presented.

### 1.4. Cardio-mechanical applications

While estimation of the LV cavity volume (and the LV geometry in general) is of direct relevance for the detection of cardiovascular diseases (Bernard et al., 2018), a fully automated approach for data extraction from images is also of interest for clinical translation of cardio-mechanical models, which is widely considered the next step for cardio-mechanical modeling (Niederer and Smith, 2016; Chabiniok et al., 2016). A particular area of interest is that of precision medicine, where patient-specific information is used to tailor treatments and decision making to each individual patient (Peirlinck et al., 2021; Mangion et al., 2018a). In this context, cardio-mechanical models can be used to provide information on the level of function of the heart, while also providing information on the causes of cardiac disease (Voorhees and Han, 2015). An important part of modeling is model calibration, where we learn a set of model parameters from measured data. This process relies on the measurement of target data, such as LV volumes, and input data, such as LV geometry. Accurate measurement techniques, combined with an accurate cardio-mechanical simulator, allow us to match a personalized cardiac model to its corresponding in vivo function (Hadjicharalambous et al., 2015; Palit et al., 2018; Gao et al., 2017b). Often for these models, the parameters have an associated physiological interpretation related to the stiffness of the material, which means that accurate estimation provides information on tissue health (Westermann et al., 2008) and allows the identification of cardiovascular diseases (Gao et al., 2017a). The translation of these practices to the clinical setting depends critically on the computational cost. Although advances have been made in the use of statistical surrogate modeling for efficient patient-specific cardio-mechanical model simulation (Noè et al., 2019; Lazarus, 2022; Davies et al., 2019), a limited number of these studies has considered the use of "automated measurement techniques", by which we mean the automatic extraction of the relevant quantities of interest (QoI) from the CMR scans. Generally, the current state-of-the-art is manual extraction, slowing down the inference process and prohibiting clinical translation. Therefore, a critical next step is a fully automated QoI extraction procedure and its use within an efficient inference framework. This is precisely the task that is tackled in the current work.

## 2. Material and method

In this study, we use cine steady-state free precession imaging to estimate the volume of the LV cavity of the patient's heart. Patient CMR scans consist of several short-axis images captured in a cardiac cycle represented by 25 to 35 time frames.

Initially, we have used deep machine learning to segment cardiac images and find parts of the image that are occupied by the LV cavity. This process has been repeated over all different short-axis slices in different time frames to make a spatio-temporal surface that represents the cross-sectional area of the left ventricle. By assuming spatio-temporal smoothness for the LV cavity shape as suggested by Yan et al. (2019), Guo et al. (2021) and Rabbani et al. (2022b) we have used a Gaussian process to fit a curved surface over the available data points. Mathematically, by integrating the surface in the direction of the medial axis of the left ventricle (longitudinally), the volume of the cavity is obtainable in each time frame. Subsequently, a stepwise regression model was used to improve the accuracy of the predictions using a set of image-based features. To demonstrate a clinical application of the estimated cavity volume, we have presented an example of inverse cardio-mechanical modeling to infer the passive stiffness of the heart muscle. In this section, each of the steps mentioned will be briefly described. Furthermore, Fig. 1 represents a summary of the data workflow of the proposed method, from the training of a deep learning model on an available CMR dataset known as ACDC (Bernard et al., 2018) to the estimation of the cavity volume of the left ventricle and myocardial passive properties.

### 2.1. Patient description

In this study, we have used 339 CMR datasets read from a group of patients presenting with ST-segment elevation myocardial infarction (MI) (clinicaltrails.gov Identifier: NCT02072850), a cohort of 111 patients recovering from COVID-19 infection, a control group of 25 patients with a high risk of cardiac disease but without a history of MI and COVID-19 (clinicaltrails.gov Identifier: NCT04403607), as well as a group of 72 healthy volunteers. Table 1 presents details of each group of patients and their population and selection criteria. The protocol used for CMR imaging was steady-state free precession cine imaging that is used to assess the LV structure and its function. For MI patients,

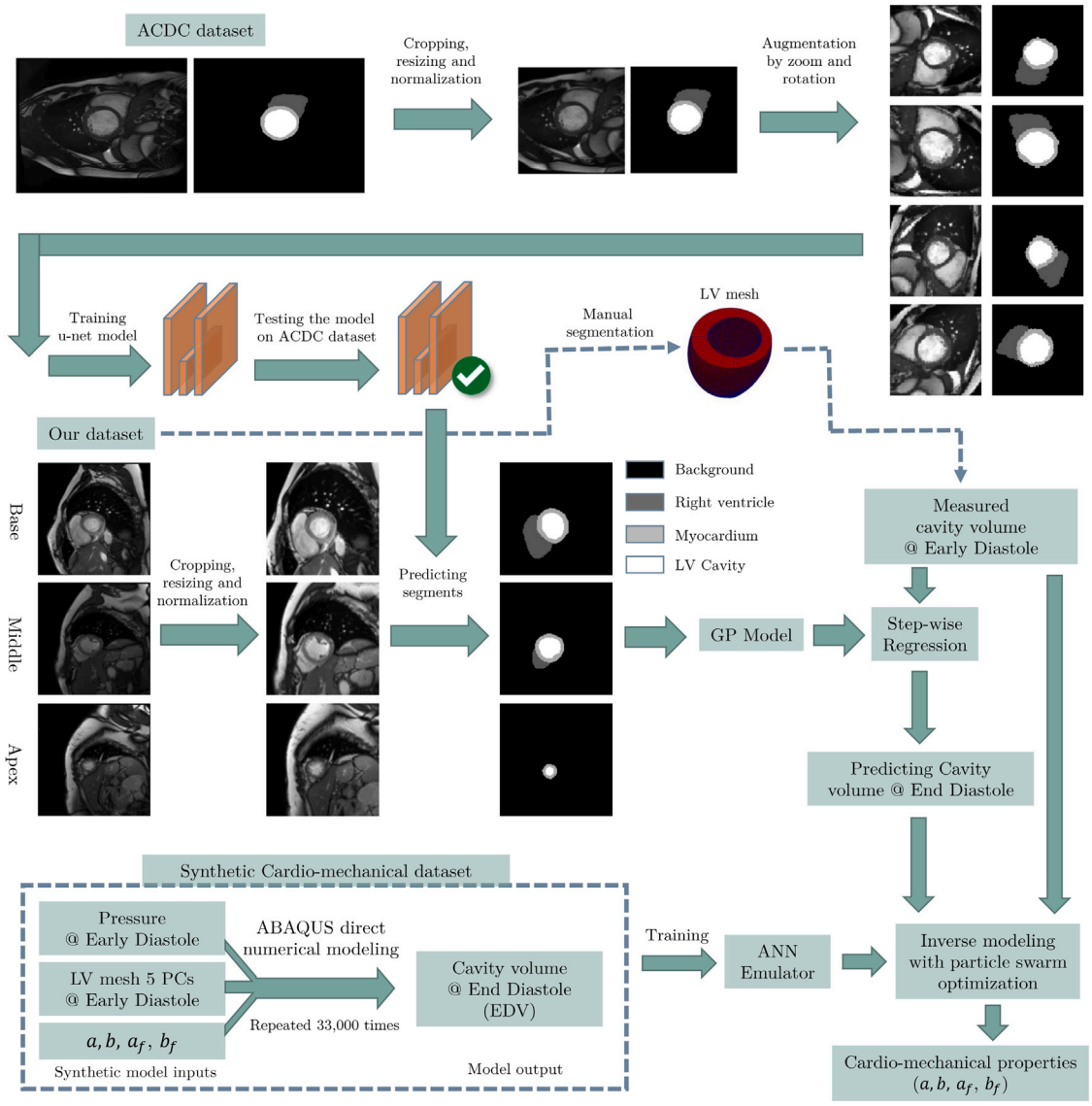


**Fig. 1.** Data processing workflow and summary of the proposed method in the present study, from building an augmented training dataset based on the ACDC dataset to predicting the left ventricle cavity volume using segmented images and estimating myocardial passive properties.

the short-axis cine scans were acquired in planes perpendicular to the LV medial axis from the base to the apex with 7 mm thickness and a 3 mm inter-slice gap. The repetition time (TR) and echo time (TE) are 1.2 ms and 3.3 ms, respectively. Furthermore, the voxel size is $1.3 \times 1.3 \times 7$ mm$^3$ and the flip angle is 80° with a bandwidth of 930 Hz/pixel. For COVID-19 study and controls, typical scan parameters were: field of view (FOV) $340 \times 286$ mm, slice thickness 7 mm with 3 mm gap in short-axis stack, repetition time (TR) 41.4 ms, echo time (TE) 1.51 ms, flip angle 50°, and voxel size $1.33 \times 1.33 \times 7$ mm. In addition to short-axis slices, standard cine images were acquired in the LV inflow and outflow tracts (LVOT), horizontal long-axis (HLA), and vertical long-axis (VLA) planes.

### 2.2. Manual segmentation

To obtain the ground truth values of the LV cavity volumes, we still rely on manual segmentation. Manual segmentation is still the current state of the art for reconstruction of ventricular geometry (Romaszko et al., 2021). In this study, we used 5 to 8 short-axis images, as well as 3 long-axis images, to perform manual segmentation at the early diastole stage of the heart using a home-made graphical user interface (GUI). It should be noted that the selection of the exact time frame in which the diastolic phase begins is done manually by finding the moment at which the mitral valve is first fully opened in the LVOT slice. The manual segmentation workflow in the developed GUI begins by asking the user to click on a series of points located on endo- and epicardium surfaces visible in short-axis images. Then, this process was repeated for 3 existing long-axis images, namely LVOT, HLA, and VLA. Afterward, through the developed GUI, the user will be asked to click on the apex point of the heart located on the endo- and epicardium surfaces, which helps with the accurate reconstruction of the LV geometry.

Due to possible movements of the patient during the imaging acquisition process, some of the CMR images could be misplaced, and in such a condition motion correction is required. For this purpose, we take the long-axis images as reference, and the user will have the option to relocate the short-axis contours to match the background long-axis image (Fig. 2-b). At this stage, two separate surfaces are automatically fitted over all endo- and epicardium contours using a cubic B-spline interpolation in a prolate spherical coordinate system (Li et al., 2020; Romaszko et al., 2021). Then the LV geometry is enclosed between the endocardial and epicardial surfaces (Fig. 2-c) consisting of 2865 quadrilateral patches and 5792 vertices (Fig. 2-d). Further details on

**Table 1**
Description of the patient groups.

| Patients group | Description | Population |
|---|---|---|
| Myocardial infarction (MI) | MI patients were selected from a population of patients with acute ST-elevation MI (STEMI), obtained within an observational study carried out between 14 July 2011 and 22 November 2012, funded by the British Heart Foundation. These patients were selected if they required percutaneous coronary intervention (PCI) due to a history of symptoms consistent with acute MI (Carrick et al., 2014). | 131 |
| COVID-19 | Patients who received hospital care for COVID-19, with or without admission, and were alive, were prospectively selected for cardio-renal MRI. MRI was acquired in a single reference site for all patients using a research-dedicated 3.0 T (3 T) scanner. All patients underwent protocol-directed MRI in the convalescent phase, 28–60 days after discharge (Berry et al., 2021). This study was funded by Chief Scientist Office. | 111 |
| COVID-19 control | The control group of patients with similar age, sex, ethnicity, and cardiovascular risk factors underwent the same research procedures as COVID-19 patients. Age range 40–80 years. At least one cardiovascular risk factor by ASSIGN criteria (Osman and Abumanga, 2019; Guzik et al., 2020). | 25 |
| Healthy volunteers (HV) | Healthy volunteers with no prior history of cardiovascular disease were enrolled for CMR imaging. They were scanned using a 1.5 T scanner without Gadolinium enhancement. The demography of this group can be found at Mangion et al. (2016). | 72 |

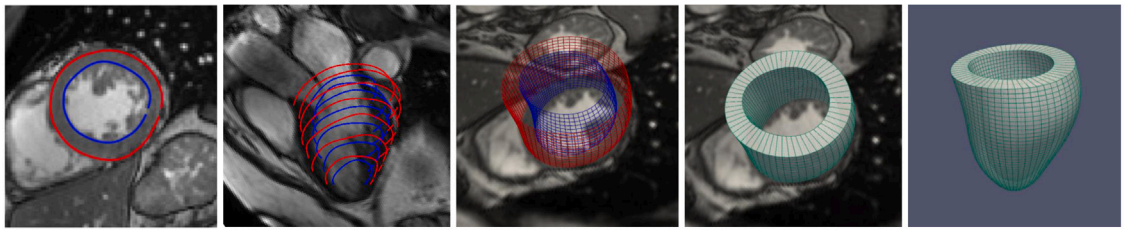


**Fig. 2.** Steps of the manual segmentation process: (a) manually adjusted endo- and epicardial cubic B-splines on a short-axis slice shown with blue and red colors, respectively, (b) motion correction for all short-axis images in reference to long-axis images, in this case, the LVOT slice, (c) fitted surfaces of endo- and epicardium, (d) the final generated LV mesh representing the myocardium overlapped with a short-axis image, (e) the final LV mesh.

manual segmentation and motion correction can be found in Gao et al. (2017b) and Li et al. (2020). The final reconstructed mesh (Fig. 2-e) can be used for an accurate calculation of the volume of the LV cavity, enclosed by the endocardial surface. Furthermore, this LV geometry can also be used as an input for cardio-mechanical simulations (Lazarus et al., 2022b; Romaszko et al., 2021).

Manual segmentation of COVID-19 patients was performed by 3 different trained operators over 6 months. In such a condition, inter- and intra-operator variability may affect the validity of the ground truth data. To estimate the amount of uncertainty in manual segmentation, CMR scans of 6 COVID-19 patients were selected to be processed by different operators, as well as the same operator repeatedly at different times. From this set of independent and repetitive manual segmentations, LV cavity volumes were computed and used for our uncertainty quantification (Fig. 9-d).

### 2.3. Deep learning segmentation

Deep learning semantic segmentation of short-axis CMR images has been performed based on a publicly available cine image dataset known as the Automated Cardiac Diagnosis Challenge (ACDC) (Bernard et al., 2018). The dataset was initially published in 2017 and its training data include CMR scans of 100 patients with 5 groups of normal, myocardial infarction, dilated cardiomyopathy, hypertrophic cardiomyopathy, and dilated right ventricle. This dataset contains manual segmentations of different elements within the CMR images, including the myocardium, the LV cavity, and the right ventricle at the end of diastole and the end of systole. The structure of the deep learning model that we have used for segmentation is known as the U-net, which has been used repeatedly for medical image segmentation and resolution enhancement in the literature (Li et al., 2018; Zhou et al., 2018; Ronneberger et al., 2015; Ankenbrand et al., 2021; Pain et al., 2022; Rabbani and Babaei, 2022; Rabbani et al., 2022a). To improve the accuracy of segmentation, as suggested in the literature (Xia and Kulis, 2017), we have used two U-net structures in a sequential manner as depicted in Fig. 3. Since the training and prediction datasets have been obtained from two different sources, the transferability of the learned patterns is challenging. In particular, CMR images that are captured from a different cohort of patients can have explicit or implicit variations that hinder transfer learning. For example, using only a dataset of overweight patients for training could lead to an overestimation of the LV volume when applied to other patients who are not overweight. In another example, training on a dataset of MI patients and predicting on a dataset of healthy volunteers may lead to an underestimation of the ejection fraction due to the bias inherent in the training data. To overcome this limitation, we have artificially augmented the ACDC dataset into a more diversified set of images so that the trained model would not be sensitive when switching between the datasets for prediction purposes. Data augmentation has been carried out using the common technique of zooming and rotation (Ankenbrand et al., 2021). Through this approach, we have augmented the 100 patients available from the ACDC dataset into 1000 instances and trained a deep neural network based on 80% of short-axis slices from the end-diastole and end-systole phases of the patient's heart. As a practical aside, we note that the deep learning model has been developed using the Python programming language based on the TensorFlow package with Keras back-end (Abadi et al., 2016). In the deep learning model and within each of the U-net structures, four stages of downsampling are implemented to decrease the dimension of the input short-axis images and detect the identity of each element in the image. Then, four sequential upsampling stages are implemented to assign the detected identities to the corresponding pixels in the output image. At each of the down-sampling stages, a 3 by 3 matrix convolution is applied using the same size output condition, and a 2 by 2 max-pooling layer with unit stride is used to shrink the size of the image by half at each of the stages. The "Exponential Linear Unit" (ELU) activation function is applied after each convolution and the filters are initialized via *He Normal* method as suggested in the original U-net structure (Ronneberger et al., 2015). Finally, to train

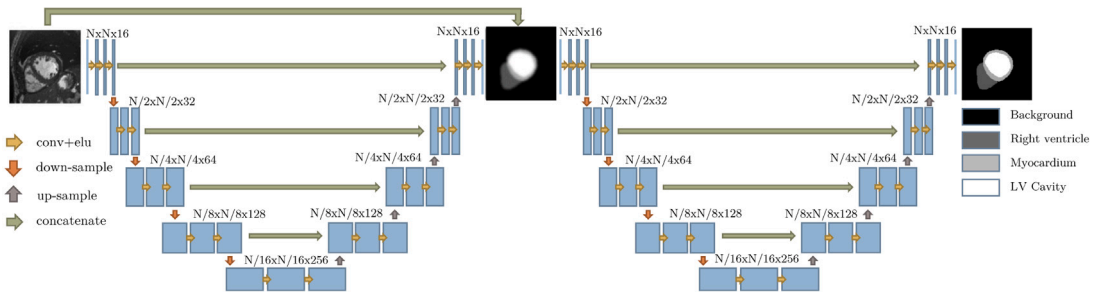


**Fig. 3.** Structure of the deep learning model used for semantic segmentation of the short-axis images of cardiac MRI. The output image background is presented by black, the right ventricle with dark gray, the myocardium with light gray, and the left ventricle cavity is shown by white pixels. Conv+elu stands for convolutional layer with exponential linear unit of activation. Also, $N$ denotes the length and height of the input image in pixels, which is equal to 256 for the present study. Blue boxes schematically show the shape of the data at each stage of the down- and up-sampling with dimensions written at the top of the boxes. For more information regarding the deep learning model structure, refer to Ronneberger et al. (2015).

the model, we have used a categorical cross-entropy loss function to penalize incorrect segmentations. It should be noted that the second U-net structure has been trained by taking the output of the first trained U-net as input to make the final prediction. Such a coupling approach helps to minimize the need for post-processing steps such as removing isolated pixels and filling empty holes in the labeled image. Fig. 3 illustrates the structure of the deep learning model used to segment the short-axis CMR images.

### 2.4. Gaussian process

When segmented images of the LV cavity are obtained, the simplest approach that can be used to estimate the volume of the cavity is counting the number of pixels and multiplying them by the physical dimensions of the pixel and the thickness of each slice in the long-axis direction. Although this simplified approach has been used repeatedly in the literature (Isensee et al., 2017; Khened et al., 2019; Ammar et al., 2021), it is not the most accurate method considering the fact that it does not take into account the 3D geometry of the left ventricle. Furthermore, this slice stacking approach must be performed manually when dealing with realistic data to handle repetitive slices at the same location, missing slices, and scarcity of slices in the apex region. To address these issues, we have used the Gaussian process (GP) package in MATLAB 2021a to fit a surface on top of all available data points that describe the cavity cross-sectional area in different time frames. For the GP kernel function, we chose the standard squared exponential based on the smooth nature of the myocardium shape and assumed a constant prior mean (Williams and Rasmussen, 2006). All kernel parameters and the mean were inferred with maximum likelihood, using the default optimization routine in the MATLAB 2021a GP package known as the quasi-Newton approximation method (Eade and Robb, 1981). The fitted surface can be extrapolated towards the apex area until it intersects with the horizontal plane of zero cross-sectional area, as visible in Fig. 4. Using this approach, we are able to estimate the cross-sectional area at the apex region, which usually suffers from the lack of information in the CMR imaging. Finally, by integrating the area enclosed below the fitted surface ($S$) over the distance from the base of the heart to the apex ($x$), the volume of the LV cavity is calculated in each time frame (Fig. 4). Mathematically, we can assume that the fitted surface is a function of time ($t$) and location ($x$):

$$S = f(x,t). \tag{1}$$

Then, integrating over $x$ gives:

$$V(t) = \int_0^{L(t)} f(x,t)\,dx \tag{2}$$

where $f$ is the fitted surface, $t$ is the time frame, and $L(t)$ is the long-axis distance from the base to the apex in each time frame, which is obtained by intersecting $f$ with the plane of zero cross-sectional areas:

$$f(L(t),t) = 0. \tag{3}$$

Solving the above equation to determine $L(t)$ is a straightforward interpolation task considering the high resolution of the available data points on the fitted surface.

### 2.5. Step-wise regression

To make the estimated volumes one step closer to the manually measured values, we have coupled the GP-obtained volumes with several image-based features that are extracted from automatically segmented images to train a stepwise linear regression model. By training this model on 80% of the available data points, we aim to reach a lower RMSE in prediction of the early diastolic LV volumes.

Initially, we have extracted 9 features related to the cross-sectional area, the cumulative distance value, and the maximum distance value of different elements in each segmented short-axis image. Distance values are pixels of a distance map that are easily computable using standard available image processing tools, including the MATLAB image processing toolbox. The distance map of a binary image shows the minimum Euclidean distance between each of the non-zero pixels to the closest zero pixel (Figs. 4–5) (Fabbri et al., 2008; Kumar and Bhatia, 2014). In the context of cardiac image segmentation, if we assign the value of one to the pixels of the object we aim to characterize and zero to the background pixels, the subsequent distance map can be treated as a shape-dependent feature. Fig. 5 illustrates the above-mentioned 9 initial features obtained from the segmented map of a short-axis slice. Features 1 to 3 show the cross-sectional area of the LV cavity, myocardium, and right ventricle, respectively. As a relevant feature, if we calculate the total number of non-zero pixels in each of these images or perform 2-D summation on the images and multiply it by the physical dimension of the pixels as well as the physical distance between each pair of slices, the outcome would be a rough estimation of the volume of an element such as left ventricle cavity. To go further in feature engineering, Euclidean distance maps of each of the heart elements are calculated in features 4 to 9. Summation of the distance map values returns a shape-related feature that may be useful for distinguishing between different hearts. Moreover, related to features 7 to 9, the maximum value of a distance map is equivalent to the radius of the largest inscribed circle inside the binary image, and it can be used as a measure to compare the thickness of the heart elements such as myocardium. Taking into account that the number of short-axis slices changes from patient to patient, a combination of averaging and the standard deviation is used to reduce the dimensionality of features across different slices (Fig. 6). A relatively similar set of features has also been used in the literature to diagnose cardiac diseases based on CMR scans (Isensee et al., 2017; Khened et al., 2019). Finally, the

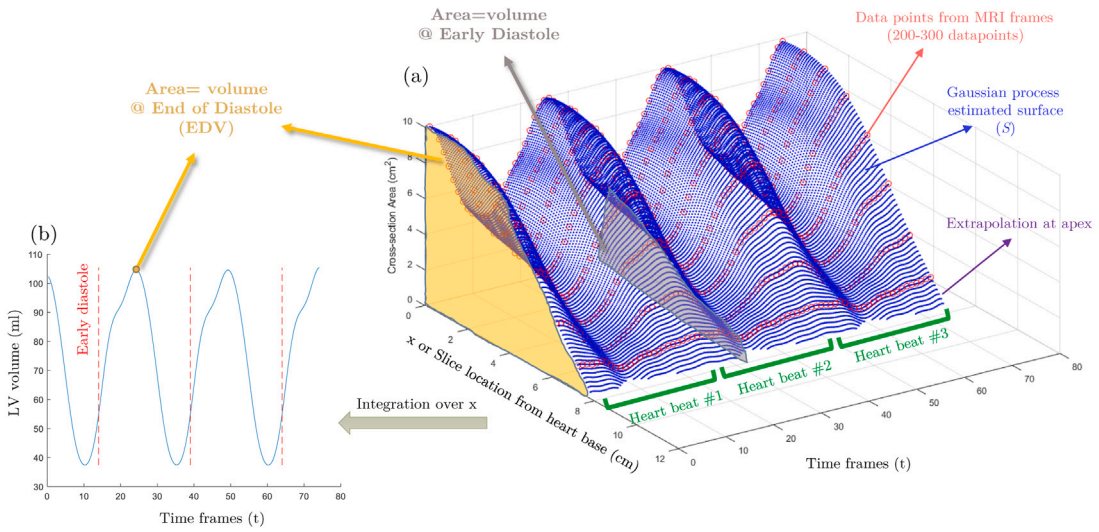


**Fig. 4.** Application of GP model fitting for improving the accuracy of left ventricle volume estimation. Panel (a): Gaussian process fitted surface over available data points of cross-sectional area of the left ventricle in different distances from the heart base. Panel (b): integrating the area enclosed below the surface (S) over the distance from the base to the apex (slice location: x) to calculate the left ventricle cavity volume at every time frame. Note that we have stacked the data points of three heart beats together, as a simple way to force a periodic boundary condition to the middle beat.

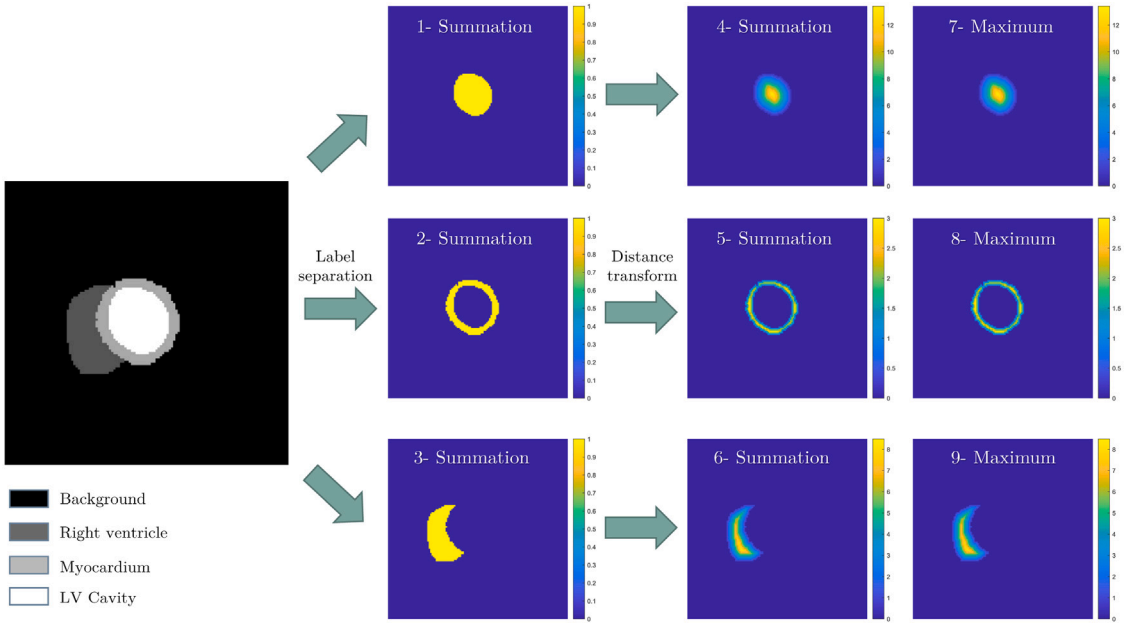


**Fig. 5.** Image-based initial features extracted from each of the short-axis slices at every time step based on the deep learning segmentation output. Note that the maximum value of the distance map, which appeared in features 7 to 9, represents the radius of the maximal inscribed circle and can be interpreted as maximum thickness of the element.

volume of the LV cavity obtained from GP regression is added as the last feature. Then, to filter out insignificant features, we have used a step-wise regression approach. A step-wise linear regression method initiates a simple linear model and gradually adds or removes variables to make a parsimonious set of variables that describes the observations more accurately (Rose and McGuire, 2019). The criterion used for feature selection is the sum of squares of errors (SSE). We calculate the $p$-value for an F-test of the change in SSE that results from the addition or removal of a feature. If the $p$-value is less than 0.05, the feature is significant for the model.

### 2.6. Cardio-mechanical modeling

To demonstrate a practical application of the presented LV cavity volume estimation method, a cardio-mechanical case study is presented. In this study, we focus on the passive filling of the LV during the diastolic phase. Passive filling of the LV is a non-linear mechanical process due to the interplay between ventricular blood pressure and stiffness of the myocardium. At the beginning of diastole, it is assumed that blood pressure is zero, the unloaded state, while as we approach the end of diastole, the ventricular pressure increases and the myocardium is passively stretched to balance the applied pressure (Wang et al., 2013). Stiffness of the myocardium has been considered a potential biomarker to characterize diastolic dysfunction, while inferring myocardial stiffness non-invasively is still a challenging research problem (Gao et al., 2017b; Borowska et al., 2022). In this study, an incompressible material model derived from the constitutive model proposed by Holzapfel and Ogden (2009) is used, that is

$$\Psi = \frac{a}{2b}[\exp\{b(I_1 - 3)\} - 1] + \sum_{i\in\{f,s\}} \frac{a_i}{2b_i}[\exp\{b_i(\max(I_{4i}, 1) - 1)^2\} - 1]$$

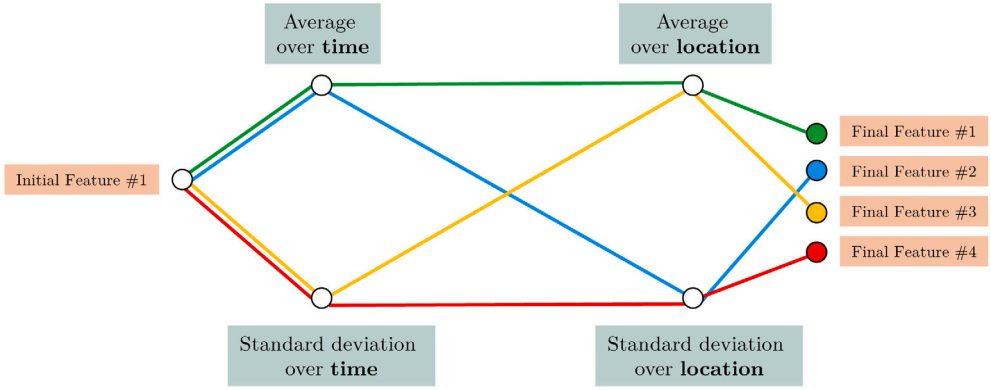


**Fig. 6.** Reducing the dimensionality of the initial features by calculating their average and standard deviation over time and slice location. Each of the initial features from Fig. 5 converts to four final features.

$$+\frac{a_{fs}}{2b_{fs}}\{\exp(b_{fs}I_{8fs}^2)-1\}, \tag{4}$$

where $a$, $b$, $a_f$, $b_f$, $a_s$, $b_s$, $a_{fs}$, and $b_{fs}$ are material constants describing the stiffness of the myocardium. In this equation, the two most significant parameters are $a$ and $b$, which are related to the isotropic response of the myocardium, while $a_f$ and $b_f$ as the second set of significant parameters describe the reinforced stiffness along myofibres (Lazarus et al., 2022a). The LV passive filling is mathematically formulated as a quasi-static pressure-loaded boundary-value problem, which can be solved numerically using finite element packages, e.g. ABAQUS (Simulia, Providence, RI, USA). For more details on this LV model, see Wang et al. (2013).

An inverse problem is usually formulated to infer material parameters in Eq. (4) by matching the model predictions to the measured data, as we observe from CMR scans (Gao et al., 2015). The search for optimal parameters can be computationally intensive due to the multi-modality of the inverse problem and the high computational costs of iterative numerical solutions of the LV model using the finite element method (Borowska et al., 2022). To avoid this issue, a statistical emulator can be trained to replace the computationally expensive LV model, reducing computational costs by several orders of magnitude; see Noè et al. (2019). The emulator model we have used is a single layer artificial neural network with 100 nodes in the hidden layer and ReLU activation. The input space of the model consists of 10 parameters, including end-diastolic pressure (EDP), 5 principal components of the LV mesh at the unloaded state (early-diastole), as explained in the next paragraph, and 4 constitutive parameters ($a$, $b$, $a_f$, $b_f$) in Eq. (4) (Fig. 1). The remaining parameters in Eq. (4) have been kept fixed at nominal values, based on our previous global sensitivity analysis study (Lazarus et al., 2022a). The output of our emulator is the end-diastolic LV volume (in mL), which feeds into the objective function Eq. (5), as discussed below.

To make a robust emulator, a large dataset of numerical simulations by running the forward ABAQUS LV model has been prepared with 33,289 entries. The data used to train the emulator were obtained from multiple different previous studies, with different material parameter distributions. The first 21,388 data points were designed using a Sobol sequence, and then the remainder of the input data points were sampled from a Beta distribution with parameters of $\alpha = 1$ and $\beta = 1.4$. The skewed Beta distribution gives a slightly increased density of points for decreasing material parameter values. This choice of distribution was based on the findings from Lazarus (2022), who showed that the function shows a more complex behavior around smaller parameter values. Expert knowledge was used to guide the choice of bounds for the material parameters. In addition to the constitutive parameters, the cardio-mechanical model takes as input the patient-specific shape of the LV at early diastole, represented by a high-dimensional (in the order of 17k) mesh of finite element nodes. To be feasible for emulation, dimension reduction is essential. In a previous study (Romaszko et al., 2019) we have shown that principal component analysis (PCA) is as accurate as more advanced machine learning methods at lower computational costs and that a projection of the LV mesh into the space spanned by the 5 leading principal components (PCs) provides a reasonable trade-off between emulation and reconstruction accuracy. We have used this insight for the present study to proceed as follows. For the PCA dimensions, the choice of bound was made based on the training set of LV geometries. More specifically, we used a set of MI and HV LV geometries to train the PCA model, which provides a map into the lower dimensional space. This is the space in which we designed our emulator. The training LV geometries can be projected into this lower dimensional space to obtain their 5 PC representations. Our parameter design space is within ±10% of the upper and lower bounds of PC projections for the MI and HV patient groups. We then used a Sobol sequence to fill this five-dimensional space with training points.

Out of the complete dataset, we have used 32,289 data points to train the NN model and 1000 randomly selected data points have been used for testing. The inference process to find the optimal set of material parameters is implemented using a particle swarm optimizer from the MATLAB 2021a optimization toolbox. The particle swarm is a nature-inspired global optimization algorithm introduced by Kennedy and Eberhart (Kennedy and Eberhart, 1995) suitable for finding the minimum value of a continuous nonlinear function in a bounded multi-dimensional space.

Our objective function ($f_o$) to be optimized is adopted from Klotz et al. (2006), Borowska et al. (2022) and Lazarus et al. (2022b), where a Klotz term is included to allow for the high stretch behavior of the tissue:

$$f_o = \left(\frac{V_8 - V_8^*}{V_8^*}\right)^2 + \left(\frac{V_{30} - V_{30}^{Kl}}{V_{30}^{Kl}}\right)^2, \tag{5}$$

$$V_{30}^{Kl} = V_0 + \frac{V^* - V_0}{(P^*/A)^{1/B}}, \tag{6}$$

Note that this objective function considers only the LV cavity volume, but not the circumferential strains. This simplification is motivated by the work of Lazarus (2022), who showed that the level of mismatch between the predicted and measured strains was such that these provided little additional information about the material parameters on top of what is encoded in the measured volume. $A$ and $B$ are Klotz constants taken from the literature (Klotz et al., 2006): 27.78 and 2.76, respectively. In addition, $V_{30}^{Kl}$ is Klotz predicted LV volume at the hypothetical pressure of 30 mmHg, $V_0$ is the initial cavity volume of LV obtained from the reconstructed LV geometry at early-diastole, $V_8$ is the end-diastolic cavity volume predicted by the NN emulator, $V_{30}$ is the cavity volume of LV predicted by the NN emulator at the pressure of 30 mmHg, and $V_8^*$ is the end-diastolic LV cavity volume estimated using the image-based method presented in the present paper. As has

been discussed extensively in Lazarus et al. (2022b), including the Klotz curve (Klotz et al., 2006) in the optimization process effectively introduces a constraint that reduce the degrees of freedom. In other words, the cardio-mechanical model should not only predict the correct end-diastolic *in vivo* volume at 8 mmHg, but also the extrapolated volume at 30 mmHg based on the Klotz curve (Borowska et al., 2022). However, considering the high-dimensional search space for material parameters and limited measured data, a simple reparameterization approach was adopted here assuming $a = a_f$ and $b = b_f$. This assumption reduces the complexity of the optimization further into a 2-dimensional search with less issues in non-uniqueness. This simplified assumption of $b = b_f$ has been independently adopted in the literature (Hadjicharalambous et al., 2015). We emphasize that the remit of our study is *not* to comprehensively study the inference problem of the cardiac mechanics model *per se*, but to demonstrate that our automatically extracted LV volume is suitable for estimating myocardial stiffness parameters. For a more comprehensive understanding of material parameter inference from in vivo data, please see Gao et al. (2015), Lazarus et al. (2022b,a), Borowska et al. (2022) and others Hadjicharalambous et al. (2015).

## 3. Results and discussions

### 3.1. Deep learning segmentation

In this section, the results of the deep learning segmentation are discussed, and subsequently, the cavity volume predictions will be presented and compared to the manually measured values. As shown in Fig. 1, we have used zooming and rotation to augment 80% of the available data within the ACDC data set. Then 10% of the data were used for validation and the rest were reserved as an independent test set to provide a fair measure of the model performance. For all our simulations, the training process was continued for approximately 100 epochs, based on an early-stopping criterion: we stopped the training process when the validation loss no longer decreased for 10 consecutive epochs. In this process, a fixed learning rate of 0.001 was used as input for the Adam optimizer (Kingma and Ba, 2015). Fig. 7 illustrates three examples of predicted segmentation from the test portion of the dataset, as well as the input and ground truth images. Fig. 7-a shows a successful prediction of heart labels with a dice coefficient above 0.99 for LV cavity, 0.86 for the myocardium, and 0.94 for the right ventricle. Fig. 7-b shows an interesting observation in the test dataset that demonstrates the generalization potential of the trained model. As can be seen within the marked area, the thickness of the myocardium is considered unrealistically thin in the manually segmented image, and a comparison with the input image reveals that the deep learning predicted label is more realistic than the manual segmentation. Fig. 7-c presents an overestimation of the size of the right ventricle by the deep learning model. However, by looking at the input images, the over-estimation error can be explained by the abnormal highlight on the boundary of the right ventricle. Note that the pixelized appearance of the manually segmented data is due to zoom- and rotation-based augmentation, which depreciates the image quality.

In addition to visual inspection of the segmentation, we have also calculated the dice score between the predicted and manual segmentations for all available data in the augmented test dataset. Fig. 8 illustrates the distribution of the dice score for the LV cavity, myocardium, and right ventricle of the test images. Moreover, the average and standard deviation of the dice scores are available in Table 2. As can be seen, the left ventricle cavity is the most predictable element inside the images, which is reasonable considering its clearly distinguishable circular cross-section located almost at the middle of all short-axis slices. Based on the standard deviation of the dice score, it can be said that the myocardium is the second most predictable element in the proposed model. Finally, the dice scores of the right ventricle are more scattered between 0 and 1, which means that the model has had difficulty predicting them. In several cases, we have observed that fatty tissues adjacent to the heart wall are susceptible to being incorrectly segmented and misclassified as the right ventricle, especially in overweight patients.

**Table 2**
Average and standard deviation of the dice scores of the deep learning predictions on the test portion of the data from ACDC dataset.

| Label | Average dice score | Standard deviation of dice scores |
|---|---|---|
| LV cavity | 0.96 | 0.021 |
| Myocardium | 0.84 | 0.038 |
| Right ventricle cavity | 0.79 | 0.225 |

### 3.2. Volume prediction results

After segmentation of different short-axis slices in all time frames, we have used the Gaussian process to fit a spatio-temporal surface that represents the cross-sectional area of the LV cavity (Fig. 4). This process has been repeated for all 339 patients in our dataset and a primary estimation of the left ventricle volume has been obtained by integrating over the distance from the base to the apex of the heart. Fig. 9-a presents a comparison between the estimated cavity volumes and the values that are measured based on manual segmentation before the implementation of the GP fitting. As can be seen, the root mean square error (RMSE) is more than 13 (mL) and the coefficient of determination ($R^2$) is around 0.74. Fig. 9-b shows a slight improvement in the prediction accuracy, which is achieved with the help of a fitted GP model. As can be seen, the GP improves the robustness of the predictions by limiting the negative effect of segmentation outliers. Finally, by fitting a step-wise regression model on the previously discussed set of 37 features, we have been able to get closer to manual accuracy, as illustrated in Fig. 9-c.

At this stage, to ensure that our step-wise regression method is a suitable approach for variable selection and predicting LV volumes, we have compared it with three alternative methods: Linear regression, Support vector machines, Lasso and Elastic Nets. We have quantified the performance in terms of out-of-sample RMSE and R-squared scores, using 5-fold cross-validation. As can be seen from Table 3, step-wise regression compares favorably with the alternative methods and shows the highest R-squared score when predicting the early-diastolic volume of LV. Using this approach, our lowest RMSE is around 8.22 ml at early diastole for 339 patients with different pathological conditions. Table 4 presents a list of the significant features that have been selected by the step-wise variable selection approach to parsimoniously estimate the LV cavity volume. Higher F-statistics and lower p-values indicate the higher significance of the features. However, step-wise regression does not select these significant variables in a univariate sense, based on their individual F-statistics and p-values, but within a multivariate framework, based on the improvement that a target variable makes when combined with other variables. As expected, the initial estimate of the LV volume that we have from GP modeling is the most relevant feature; however, as we can see in Fig. 9-b, it includes a considerable amount of noise that leaves room for further improvement. Thus, the next 6 features are included to make the model more robust and able to compensate for the noise in Fig. 9-b. We have used 5-fold cross-validation to fit the coefficients of the regression model, and we reached a coefficient of determination around 0.9 (Fig. 9-c). Finally, to get a rough estimate of the best practically achievable accuracy, we have investigated the inherent error that we have in finding the ground truth volume. For this purpose, 6 of the COVID-19 patients were selected by 3 operators (A.R., A.L., and D.D.), conceptually with different levels of segmentation difficulty based on image quality or controversial shape of the myocardium. Then, each patient's data was segmented by all three operators to give a sense of inter-operator variability. Afterward, each of the operators carried out the manual segmentation repeatedly on two of the samples to quantify the intra-operator variability. We have calculated an overall deviation error to evaluate our automatic machine learning method and compare it with the average manual accuracy. To quantify deviations in manually derived volumes, we have assumed that the average value of all manually derived volumes is the

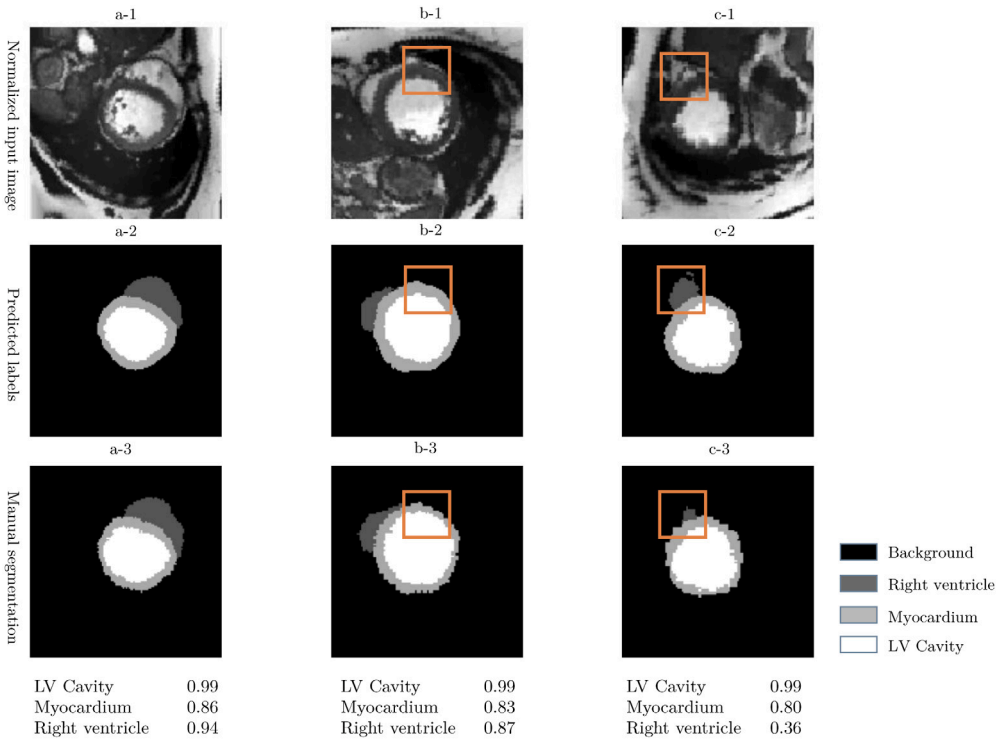


**Fig. 7.** Examples of the short-axis segmentation from the ACDC augmented test dataset, including dice scores of different elements. Panel (a): An example of a well-predicted set of labels. Panel (b): An example of the high generalization power of the deep learning model, which even beats the manually segmented images when compared with the input image. As can be seen, the thickness of the myocardium is underestimated in the manual segmentation. Panel (c): An example of the overestimation of the size of the right ventricle by the deep learning model. This can be explained by the abnormal input image with a highlight on the boundary of the right ventricle, which is difficult to interpret.

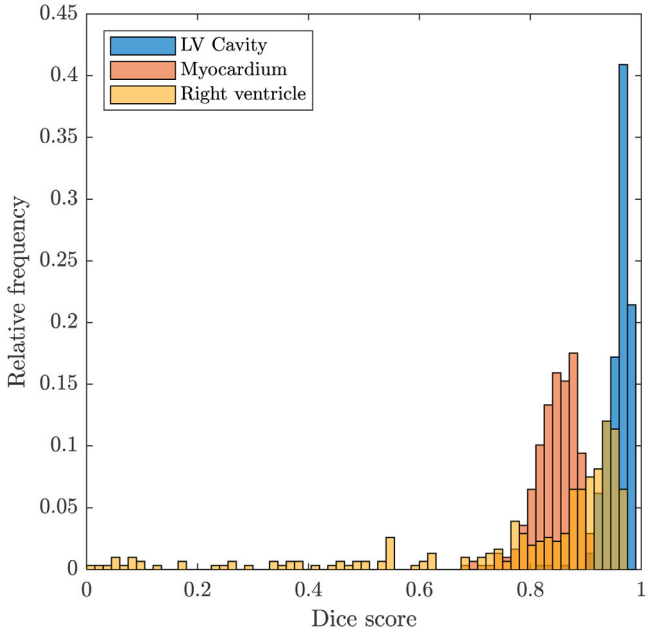


**Fig. 8.** Distribution of the dice scores in prediction of different elements of the short-axis images in the ACDC test dataset.

ground truth and compared all other volumes with the average values for a specific patient. As a result, an RMSE of 4.12 is obtained, with the coefficient of determination ($R^2$) around 0.93. This is quite close to our best automated estimation of $R^2$ equal to 0.9.

In addition to early diastole manual segmentation of 339 patients, we have manually segmented the end-diastolic images of 41 patients to ensure the applicability of the present model to the full heart cycle. The model was able to predict the end-diastolic LV cavity volume with an RMSE of 6.7 mL as presented in Fig. 10-a. We postulate that the higher accuracy in volume prediction is related to a clearer boundary between the myocardium and the cavity at end diastole in CMR cine images. Considering that the volume of the heart elements is calculated in each time frame, changes in the LV cavity volume would be an interesting parameter to observe during a cardiac cycle. Fig. 10-b illustrates these changes for 339 patients color-coded based on the LV end-diastolic volume. The relationship between the slope and curvature of the presented graphs and the pathological condition of the patients is suggested to be investigated in future studies.

### 3.3. Cardio-mechanical emulation

An artificial neural network (ANN) model has been trained as an emulator to predict the end-diastolic volume of the left ventricle. After around 1000 epochs of training using the Levenberg Marquardt (Moré, 1978) method, the model stopped showing improvement for 50 consecutive epochs. At this stage, the root mean square error (RMSE) of 1.76 mL and $R^2$ of 0.997 were achieved on the test dataset (Fig. 11). Furthermore, around 90% of the prediction residuals have been found to be smaller than ±2 (ml). Considering the low amount of error in the emulator-predicted volume compared to the manual and deep learning approaches, respectively, around 4 and 8 mL, the uncertainty of the emulator would not be a bottleneck for the inverse modeling application. While the direct numerical simulation of the diastolic phase using ABAQUS can take up to 10–20 min to run on a regular workstation, the trained emulator is able to predict the end-diastolic volume in a few milliseconds (Noè et al., 2019). Such a high prediction speed is specifically useful when the function is required to be called hundreds of times during an iterative optimization process.

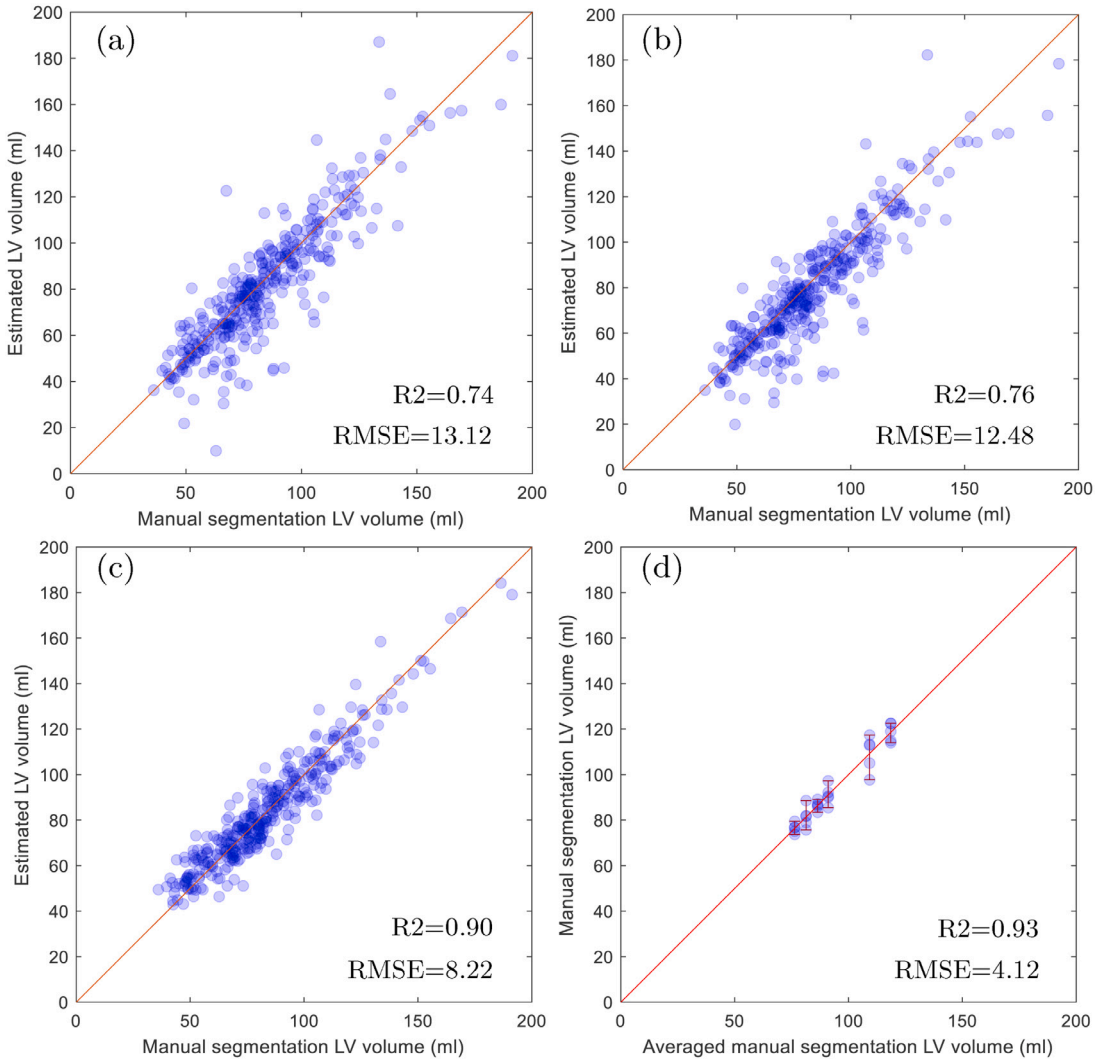


**Fig. 9.** Comparison of the manual and automated estimation methods of left ventricle cavity volume at early diastole. Panel (a): initial volume estimation without using the Gaussian process surface. Panel (b): improved volume estimation using Gaussian process surface fitting. Panel (c): further improvement of the volume estimation using Gaussian process surface fitting and step-wise regression. Panel (d): uncertainty of manual segmentation of LV cavity volume under the condition of different operators or the same operator in different attempts. Note that the axis labels in the last graph are different from the other graphs.

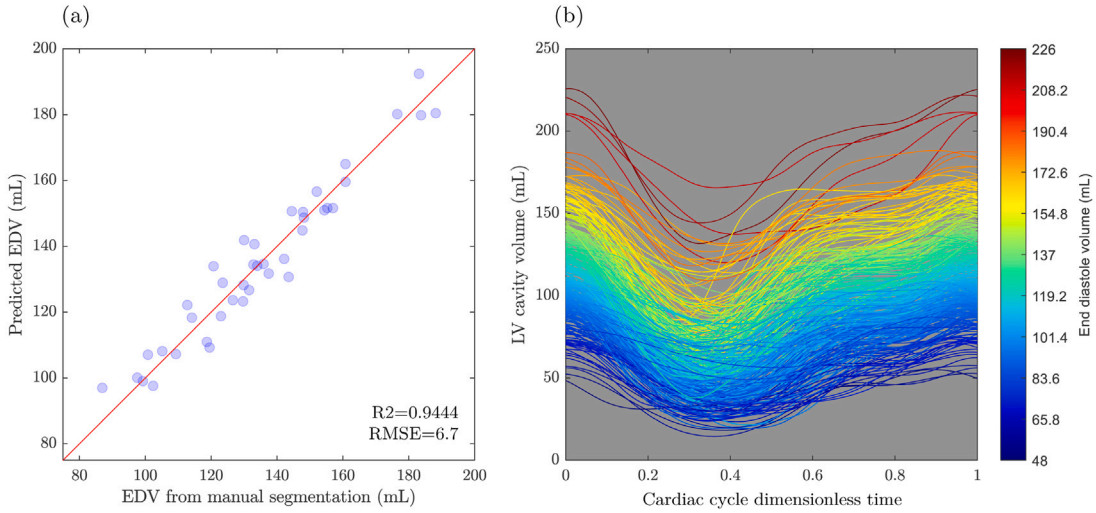


**Fig. 10.** Panel (a): prediction of the end-diastolic LV cavity volume using the proposed method in comparison with the volumes obtained based on manual segmentation. Panel (b): prediction of the LV cavity volume during the whole cardiac cycle for 339 patients, color coded based on the LV end-diastolic volume (EDV).

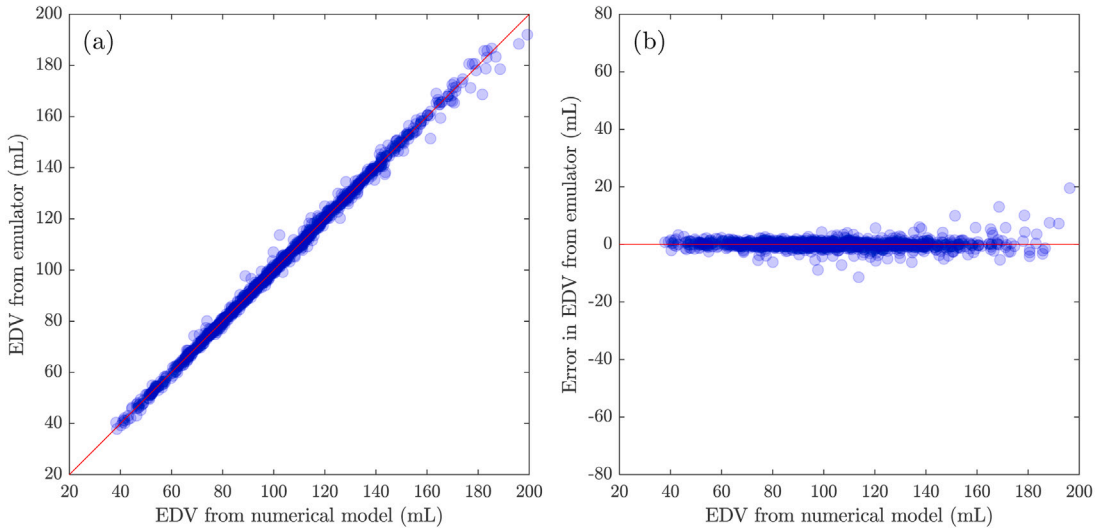


**Fig. 11.** Testing of the emulator performance for the LV diastole phase. Panel (a): EDV from the ANN emulator vs EDV from direct ABAQUS simulations with $R^2$ equal to 0.997. Panel (b): residuals of the ANN predictions with around 90% of the errors under ±2 (ml).

**Table 3**
Root mean squared error (RMSE) in LV volume and R-squared for different regression models with a 5-fold validation approach.

| Method | Settings | RMSE | R-squared |
|---|---|---|---|
| Linear regression | 5% significance level | 8.94 | 0.86 |
| Support vector machine regression | Linear kernel function | 11.4 | 0.79 |
| Lasso and Elastic Net | Weight of lasso versus ridge optimization = 0.75 | 9.83 | 0.81 |
| Step-wise linear regression | Refer to Section 2.5 | 8.22 | 0.9 |

**Table 4**
List of image-based features used to improve the estimation of the volume of the left ventricle cavity in early diastole.

| Feature rank | Feature name | F-statistics | *p*-value |
|---|---|---|---|
| 1 | LV volume initial estimate | 1394.6 | 8.1E−122 |
| 2 | Std of mean of RV volumes | 88.4 | 8.51E−19 |
| 3 | Std of mean of RV distances | 27.4 | 2.85E−07 |
| 4 | Mean of mean of RV volumes | 19.4 | 1.4E−05 |
| 5 | Mean of Std of LV volumes | 12.2 | 0.00052 |
| 6 | Mean of mean of RV distances | 15.5 | 9.63E−05 |
| 7 | Std of mean of LV thicknesses | 5.8 | 0.0163 |

### 3.4. Inverse modeling results

A particle swarm optimizer with a function tolerance of $10^{-6}$ has been used to find the constitutive parameters of the myocardium. The swarm size has been set to 20 with the maximum number of iterations equal to 400. Moreover, the minimum neighbor fraction has been set to 0.25. The mentioned parameters are set on the basis of the default values suggested in the MATLAB R2021a optimization toolbox reference manual. The objective function of optimization is described in Eq. (5). The optimization continues until a set of parameters can be found that minimizes the objective function. Fig. 12 illustrates the changes in the objective function with respect to $a$ and $b$. The optimal point lies within the oval valley formed on the response surface. In our observed cases, the formed valley has a slope towards its center, which leads to a unique set of parameters when using a global optimizer such as the particle swarm method. We have observed that for some cases, such as patient #4 in Fig. 12-d, the optimal point approaches the lower range of the parameter $a$. Considering the fact that the negative values for $a$ are not physically feasible, it is suggested that in future studies a denser parameter design with a higher coverage of smaller values needs to be used for training the emulator.

Furthermore, we have compared the mechanical parameters obtained for four patients with COVID-19 in Fig. 13 based on EDV from manual segmentation, as well as the automated approach presented in this study. If we assume that the parameters obtained based on the manual EDVs are the ground truth, for the presented four patients, the average relative errors in the prediction of $a$ and $b$ are 5.95% and 4.0%, respectively. The un-iaxial stretch–stress responses along myocytes are also shown in Fig. 13. These are produced by virtually stretching a myocardial strip along a specific direction uni-axially (Borowska et al., 2022), with tissue properties described by the selected strain energy function with given material parameter values. While both parameters influence the behavior of the myocardium at all stretch values, the stress at low stretch values is more sensitive to the value of $a$ while the stress at a high stretch is more sensitive to the value of $b$. It can be seen that the set of parameters estimated using the automated EDV has nearly identical mechanical properties as the estimated parameters from the manual EDV.

## 4. Conclusions

In the present study, we have presented a novel method for estimating the volume of the left ventricular cavity from cardiac magnetic resonance cine images of a patient's heart. In this method, we have used Gaussian process modeling to fit a spatio-temporal surface over the data points from the left ventricle cross-sectional area of the patient's heart. The fitted model can be used to estimate the cavity volume with a higher accuracy compared to the common practice in the literature and in the clinic. We have observed that the presented method decreased the RMSE of the early-diastolic volume of 339 patients from 13 to 8 mL. This improvement is valuable considering that the volume estimation based on manual segmentation as the state-of-the-art has an RMSE of around 4 mL. An accurate volume estimation method can have several clinical and biomechanical applications. An accurate estimation of the ejection fraction as a significant feature in the detection of various cardio-vascular diseases, including myocardial infarction, is a major application of the presented method. In addition, more in-depth cardio-mechanical simulations can be done by knowing the changes

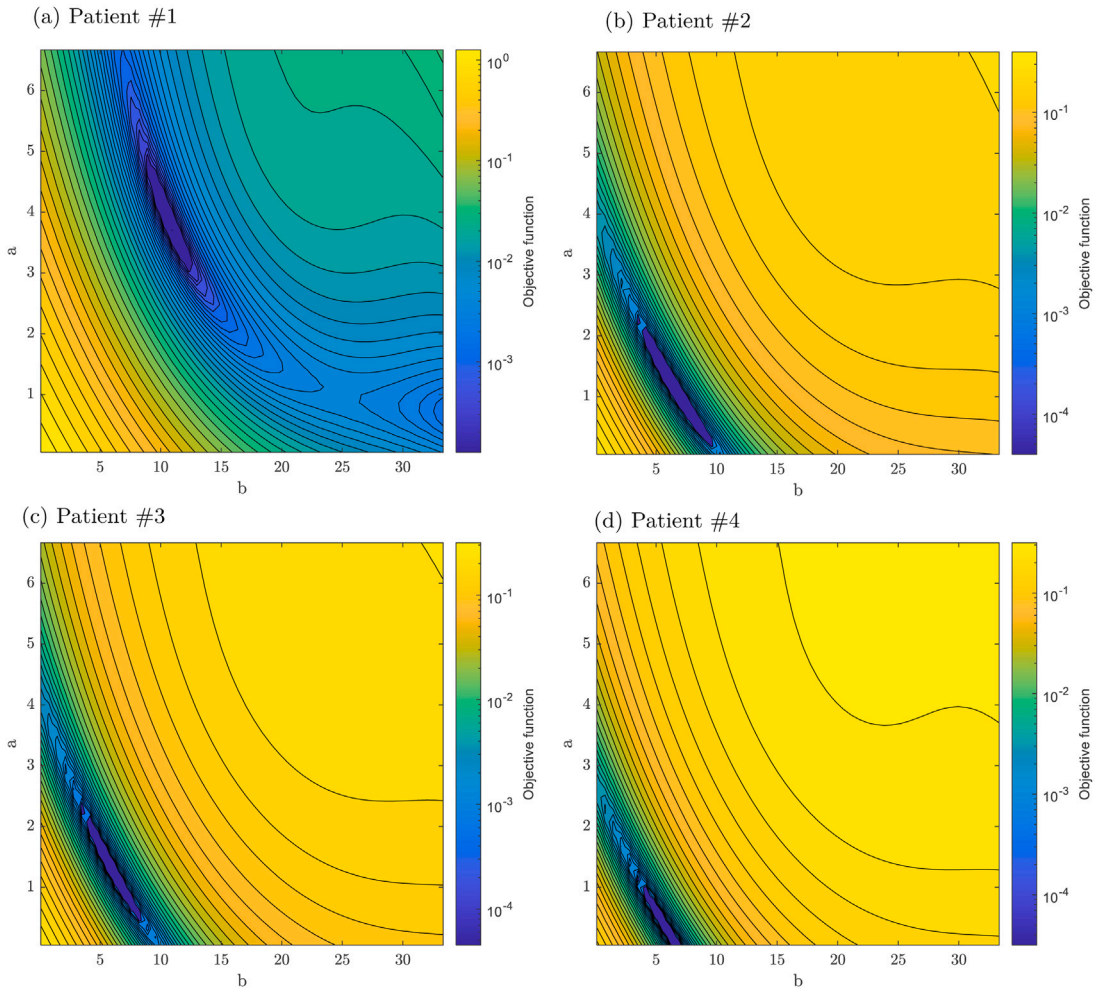


**Fig. 12.** Contour plot of the objective function as a function of $a$ and $b$, the main parameters of the Holzapfel–Ogden model, for patients #1 to#4. The location of the optimal points is available in the bar charts visualized in Fig. 13.

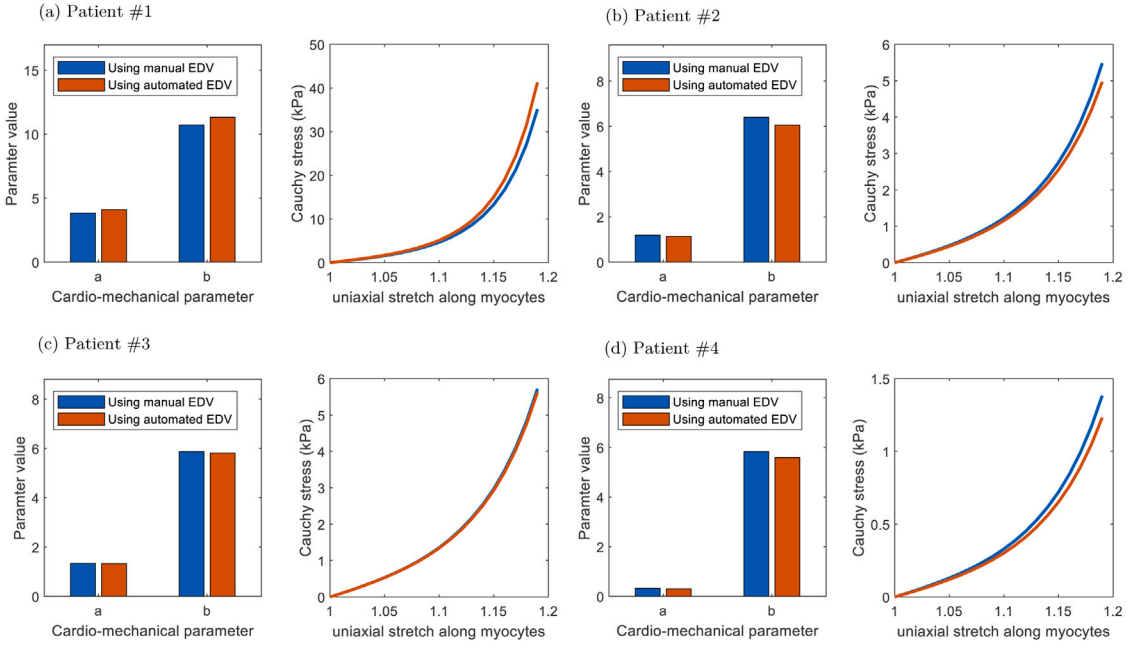


**Fig. 13.** Parameters of the Holzapfel–Ogden model from inverse modeling for patients #1 to #4 as well as the stress–stretch curves obtained based on the estimated parameters from manual and automated EDVs.

in the LV cavity volume. In this paper, we have described an inverse modeling approach that can be used to estimate important mechanical parameters of the heart by knowing the early-diastolic geometry, pressure, and the end-diastolic LV volume. Such inferred parameters are of high clinical interest as they have the potential to detect cardiac abnormalities e.g. by alerting clinicians to excessive myocardial stiffness non-invasively (Mangion et al., 2018b). In a previous study (Gao et al., 2017a), we have demonstrated that the myocardial stiffness for patients with myocardial infarction is much higher than that of healthy volunteers, where myocardial stiffness was inferred using the same material model as in Eq. (4) of our present article. The estimation of myocardial stiffness is also highly relevant to the detection of LV diastolic dysfunction, which is one of the main underlying causes of diastolic heart failure (Zile et al., 2004). Finally, the main results of the present study can be summarized as follows.

- The early diastolic volume of the LV cavity has been estimated based on the cine CMR images for 339 patients with RMSE of around 8.2 mL. Furthermore, the end-diastolic volume of the LV cavity has been estimated for 41 COVID-19 patients with RMSE of around 6.7 mL. The accuracy of these fully automated estimations is encouraging considering the 4.1 mL RMSE of manual segmentation as the state-of-the-art.
- An artificial neural network emulator has been trained to approximate the outcome of cardio-mechanical numerical simulations. The emulator predicts the end-diastolic volume of the LV with a RMSE of 1.76 mL.
- An inverse modeling approach has been implemented to estimate the mechanical properties of the myocardium ($a$ and $b$) based on the Holzapfel–Ogden myocardial model, with a relative error of 5.95% and 4.0% in estimated $a$ and $b$, respectively. In addition, the uni-axial Cauchy stress of the myocardium along myocytes has been estimated with an average relative error of approximately 6.1% compared to the condition that all volume measurements are estimated based on manual segmentation.

## 5. Limitations

The proposed method is based on 2-D short-axis CMR scans; long-axis images, which may contain potentially important complementary information about the geometry of the left ventricle, have not been included in this work, as found in our previous study in which the accuracy of the LV geometry reconstruction could be improved by including long-axis images using a deep learning approach (Romaszko et al., 2021).

In addition, the lack of information from the apex zone of the LV may lead to some errors in the estimation of LV volume. We intend to include long-axis images in our future studies to compensate for this limitation. Furthermore, we have not corrected for potential motion artifacts that may result from a patient's movement or their failure to hold their breath during the MRI scan. Finally, the reparameterization of the mechanical model of the myocardium that was used in our study may affect the accuracy of the estimated stiffness. In our future work, we plan to use a time series of LV deformations at different stages in the diastolic phase, which we expect will improve the identifiability of cardiac mechanic parameters.

## CRediT authorship contribution statement

**Arash Rabbani:** Conceptualization, Methodology, Software, Writing – original draft. **Hao Gao:** Writing – review & editing, Supervision. **Alan Lazarus:** Software, Writing – original draft. **David Dalton:** Software, Writing – original draft. **Yuzhang Ge:** Software. **Kenneth Mangion:** Reviewing & editing. **Colin Berry:** Reviewing & editing. **Dirk Husmeier:** Writing – review & editing, Supervision.

## Declaration of competing interest

The authors declare that they have no known competing financial interests or personal relationships that could have appeared to influence the work reported in this paper.

## Data availability

Left ventricle volume estimation code is publicly available at https://github.com/ArashRabbani/VentricleVolume.

## Acknowledgment

The authors express their gratitude to EPSRC (EP/S020950/1) and British Heart Foundation for funding this work (grant reference numbers EP/T017899/1, EP/R511705/1, and RE/18/634217).

## References

Abadi, M., Barham, P., Chen, J., Chen, Z., Davis, A., Dean, J., Devin, M., Ghemawat, S., Irving, G., Isard, M., et al., 2016. {Tensorflow}: A system for {large-scale} machine learning. In: 12th USENIX Symposium on Operating Systems Design and Implementation (OSDI 16). pp. 265–283.

Ammar, A., Bouattane, O., Youssfi, M., 2021. Automatic cardiac cine MRI segmentation and heart disease classification. Comput. Med. Imaging Graph. 88, 101864.

Ankenbrand, M.J., Lohr, D., Schlötelburg, W., Reiter, T., Wech, T., Schreiber, L.M., 2021. Deep learning-based cardiac cine segmentation: Transfer learning application to 7T ultrahigh-field MRI. Magn. Reson. Med. 86 (4), 2179–2191.

Bernard, O., Lalande, A., Zotti, C., Cervenansky, F., Yang, X., Heng, P.-A., Cetin, I., Lekadir, K., Camara, O., Ballester, M.A.G., et al., 2018. Deep learning techniques for automatic MRI cardiac multi-structures segmentation and diagnosis: is the problem solved? IEEE Trans. Med. Imaging 37 (11), 2514–2525.

Berry, C., Morrow, A., Sykes, R., McIntosh, A., Kamdar, A., Bagot, C., Barrientos, P., Bayes, H., Blyth, K., Briscoe, M., et al., 2021. Post-COVID-19 illness trajectory: a multisystem investigation (preprint). Res. Sq..

Borowska, A., Gao, H., Lazarus, A., Husmeier, D., 2022. Bayesian optimisation for efficient parameter inference in a cardiac mechanics model of the left ventricle. Int. J. Numer. Methods Biomed. Eng. e3593.

Bucciarelli-Ducci, C., Ostenfeld, E., Baldassarre, L.A., Ferreira, V.M., Frank, L., Kallianos, K., Raman, S.V., Srichai, M.B., McAlindon, E., Mavrogeni, S., et al., 2020. Cardiovascular disease in women: insights from magnetic resonance imaging. J. Cardiovasc. Magn. Reson. 22 (1), 1–17.

Carrick, D., Oldroyd, K.G., McEntegart, M., Haig, C., Petrie, M.C., Eteiba, H., Hood, S., Owens, C., Watkins, S., Layland, J., et al., 2014. A randomized trial of deferred stenting versus immediate stenting to prevent no-or slow-reflow in acute ST-segment elevation myocardial infarction (DEFER-STEMI). J. Am. Coll. Cardiol. 63 (20), 2088–2098.

Chabiniok, R., Wang, V.Y., Hadjicharalambous, M., Asner, L., Lee, J., Sermesant, M., Kuhl, E., Young, A.A., Moireau, P., Nash, M.P., Chapelle, D., Nordsletten, D.A., 2016. Multiphysics and multiscale modelling, data-model fusion and integration of organ physiology in the clinic: ventricular cardiac mechanics. In: Interface Focus. pp. 1–24.

Chen, C., Qin, C., Qiu, H., Tarroni, G., Duan, J., Bai, W., Rueckert, D., 2020. Deep learning for cardiac image segmentation: A review. Front. Cardiovasc. Med. 7, http://dx.doi.org/10.3389/fcvm.2020.00025, URL https://www.frontiersin.org/articles/10.3389/fcvm.2020.00025.

Dalton, D., Lazarus, A., Rabbani, A., Gao, H., Husmeier, D., 2021. Graph neural network emulation of cardiac mechanics. In: Proceedings of the 3 Rd International Conference on Statistics: Theory and Applications. 127–1–127–8.

Davies, V., Noè, U., Lazarus, A., Gao, H., Macdonald, B., Berry, C., Luo, X., Husmeier, D., 2019. Fast parameter inference in a biomechanical model of the left ventricle by using statistical emulation. J. R. Stat. Soc. Ser. C. Appl. Stat. 68 (5), 1555–1576. http://dx.doi.org/10.1111/rssc.12374, arXiv:https://rss.onlinelibrary.wiley.com/doi/pdf/10.1111/rssc.12374. URL https://rss.onlinelibrary.wiley.com/doi/abs/10.1111/rssc.12374.

Duan, J., Bello, G., Schlemper, J., Bai, W., Dawes, T.J.W., Biffi, C., de Marvao, A., Doumoud, G., O'Regan, D.P., Rueckert, D., 2019. Automatic 3D bi-ventricular segmentation of cardiac images by a shape-refined multi- task deep learning approach. IEEE Trans. Med. Imaging 38 (9), 2151–2164. http://dx.doi.org/10.1109/TMI.2019.2894322.

Eade, R.H., Robb, M.A., 1981. Direct minimization in mc scf theory. The quasi-newton method. Chem. Phys. Lett. 83/2, 362–368.

Fabbri, R., Costa, L.D.F., Torelli, J.C., Bruno, O.M., 2008. 2D euclidean distance transform algorithms: A comparative survey. ACM Comput. Surv. 40 (1), 1–44.

Gao, H., Aderhold, A., Mangion, K., Luo, X., Husmeier, D., Berry, C., 2017a. Changes and classification in myocardial contractile function in the left ventricle following acute myocardial infarction. J. R. Soc. Interface 14 (132), 20170203.

Gao, H., Li, W., Cai, L., Berry, C., Luo, X., 2015. Parameter estimation in a Holzapfel–Ogden law for healthy myocardium. J. Eng. Math. 95 (1), 231–248.

Gao, H., Mangion, K., Carrick, D., Husmeier, D., Luo, X., Berry, C., 2017b. Estimating prognosis in patients with acute myocardial infarction using personalized computational heart models. Sci. Rep. 7 (1), 1–14.

Guo, Y., Bi, L., Zhu, Z., Feng, D.D., Zhang, R., Wang, Q., Kim, J., 2021. Automatic left ventricular cavity segmentation via deep spatial sequential network in 4D computed tomography. Comput. Med. Imaging Graph. 91, 101952.

Guzik, T.J., Mohiddin, S.A., Dimarco, A., Patel, V., Savvatis, K., Marelli-Berg, F.M., Madhur, M.S., Tomaszewski, M., Maffia, P., D'acquisto, F., et al., 2020. COVID-19 and the cardiovascular system: implications for risk assessment, diagnosis, and treatment options. Cardiovasc. Res. 116 (10), 1666–1687.

Hadjicharalambous, M., Chabiniok, R., Asner, L., Sammut, E., Wong, J., Carr-White, G., Lee, J., Razavi, R., Smith, N., Nordsletten, D., 2015. Analysis of passive cardiac constitutive laws for parameter estimation using 3D tagged MRI. Biomech. Model. Mechanobiol. 14 (4), 807–828.

van Hamersvelt, R.W., Zreik, M., Voskuil, M., Viergever, M.A., Išgum, I., Leiner, T., 2019. Deep learning analysis of left ventricular myocardium in CT angiographic intermediate-degree coronary stenosis improves the diagnostic accuracy for identification of functionally significant stenosis. Eur. Radiol. 29 (5), 2350–2359. http://dx.doi.org/10.1007/s00330-018-5822-3.

Heidenreich, P.A., Trogdon, J.G., Khavjou, O.A., Butler, J., Dracup, K., Ezekowitz, M.D., Finkelstein, E.A., Hong, Y., Johnston, S.C., Khera, A., et al., 2011. Forecasting the future of cardiovascular disease in the United States: a policy statement from the American heart association. Circulation 123 (8), 933–944.

Hernandez, K.A.L., Rienmüller, T., Baumgartner, D., Baumgartner, C., 2021. Deep learning in spatiotemporal cardiac imaging: A review of methodologies and clinical usability. Comput. Biol. Med. 130, 104200.

Holzapfel, G.A., Ogden, R.W., 2009. Constitutive modelling of passive myocardium: a structurally based framework for material characterization. Phil. Trans. R. Soc. A 367 (1902), 3445–3475.

Isensee, F., Jaeger, P.F., Full, P.M., Wolf, I., Engelhardt, S., Maier-Hein, K.H., 2017. Automatic cardiac disease assessment on cine-MRI via time-series segmentation and domain specific features. In: International Workshop on Statistical Atlases and Computational Models of the Heart. Springer, pp. 120–129.

Kennedy, J., Eberhart, R., 1995. Particle swarm optimization. In: Proceedings of ICNN'95-International Conference on Neural Networks, vol. 4. IEEE, pp. 1942–1948.

Khened, M., Alex, V., Krishnamurthi, G., 2018. Densely connected fully convolutional network for short-axis cardiac cine MR image segmentation and heart diagnosis using random forest. In: Pop, M., Sermesant, M., Jodoin, P.-M., Lalande, A., Zhuang, X., Yang, G., Young, A., Bernard, O. (Eds.), Statistical Atlases and Computational Models of the Heart. ACDC and MMWHS Challenges. Springer International Publishing, Cham, pp. 140–151.

Khened, M., Kollerathu, V.A., Krishnamurthi, G., 2019. Fully convolutional multi-scale residual DenseNets for cardiac segmentation and automated cardiac diagnosis using ensemble of classifiers. Med. Image Anal. 51, 21–45.

Kingma, D.P., Ba, J., 2015. ADAM: A method for stochastic optimization 3rd International Conference on Learning Representations, {ICLR} 2015, San Diego, CA, USA, May 7–9, 2015, Conference Track Proceedings. In: Conference Track Proceedings, pp. 1–15.

Klotz, S., Hay, I., Dickstein, M.L., Yi, G.-H., Wang, J., Maurer, M.S., Kass, D.A., Burkhoff, D., 2006. Single-beat estimation of end-diastolic pressure-volume relationship: a novel method with potential for noninvasive application. Am. J. Physiol. Heart Circ. Physiol. 291 (1), H403–H412.

Kumar, G., Bhatia, P.K., 2014. A detailed review of feature extraction in image processing systems. In: 2014 Fourth International Conference on Advanced Computing & Communication Technologies. IEEE, pp. 5–12.

Lazarus, A., 2022. Surrogate modelling of a patient-specific mathematical model of the left ventricle in diastole (Ph.D. thesis). University of Glasgow.

Lazarus, A., Dalton, D., Husmeier, D., Gao, H., 2022a. Sensitivity analysis and inverse uncertainty quantification for the left ventricular passive mechanics. Biomech. Model. Mechanobiol. 1–30.

Lazarus, A., Gao, H., Luo, X., Husmeier, D., 2022b. Improving cardio-mechanic inference by combining in vivo strain data with ex vivo volume-pressure data. J. R. Stat. Soc. Ser. C. Appl. Stat..

Li, X., Chen, H., Qi, X., Dou, Q., Fu, C.-W., Heng, P.-A., 2018. H-DenseUNet: hybrid densely connected UNet for liver and tumor segmentation from CT volumes. IEEE Trans. Med. Imaging 37 (12), 2663–2674.

Li, W., Gao, H., Mangion, K., Berry, C., Luo, X., 2020. Apparent growth tensor of left ventricular post myocardial infarction–In human first natural history study. Comput. Biol. Med. 129, 104168.

Liu, X., Fan, Y., Li, S., Chen, M., Li, M., Hau, W.K., Zhang, H., Xu, L., Lee, A.P.-W., 2021. Deep learning-based automated left ventricular ejection fraction assessment using 2-D echocardiography. Am. J. Physiol. Heart Circ. Physiol. 321 (2), H390–H399. http://dx.doi.org/10.1152/ajpheart.00416.2020, Publisher: American Physiological Society. URL https://journals.physiology.org/doi/full/10.1152/ajpheart.00416.2020.

Mangion, K., Gao, H., Husmeier, D., Luo, X., Berry, C., 2018a. Advances in computational modelling for personalised medicine after myocardial infarction. Heart (British Cardiac Society) 104 (7), 550—557. http://dx.doi.org/10.1136/heartjnl-2017-311449.

Mangion, K., Gao, H., Husmeier, D., Luo, X., Berry, C., 2018b. Advances in computational modelling for personalised medicine after myocardial infarction. Heart 104 (7), 550–557.

Mangion, K., Gao, H., McComb, C., Carrick, D., Clerfond, G., Zhong, X., Luo, X., Haig, C.E., Berry, C., 2016. A novel method for estimating myocardial strain: assessment of deformation tracking against reference magnetic resonance methods in healthy volunteers. Sci. Rep. 6 (1), 1–8.

Mangold, S., Kramer, U., Franzen, E., Erz, G., Bretschneider, C., Seeger, A., Claussen, C., Niess, A., Burgstahler, C., 2013. Detection of cardiovascular disease in elite athletes using cardiac magnetic resonance imaging. In: RÖFo-Fortschritte Auf Dem Gebiet Der RÖNtgenstrahlen Und Der Bildgebenden Verfahren. 185/12, © Georg Thieme Verlag KG, pp. 1167–1174.

Moré, J.J., 1978. The levenberg-marquardt algorithm: implementation and theory. In: Numerical Analysis. Springer, pp. 105–116.

Niederer, S.A., Smith, N.P., 2016. Using physiologically based models for clinical translation: predictive modelling, data interpretation or something in-between? J. Physiol. 594 (23), 6849–6863. http://dx.doi.org/10.1113/JP272003, arXiv:https://physoc.onlinelibrary.wiley.com/doi/pdf/10.1113/JP272003. URL https://physoc.onlinelibrary.wiley.com/doi/abs/10.1113/JP272003.

Noè, U., Lazarus, A., Gao, H., Davies, V., Macdonald, B., Mangion, K., Berry, C., Luo, X., Husmeier, D., 2019. Gaussian process emulation to accelerate parameter estimation in a mechanical model of the left ventricle: a critical step towards clinical end-user relevance. J. R. Soc. Interface 16 (156), 20190114.

O'Dell, W.G., 2019. Accuracy of left ventricular cavity volume and ejection fraction for conventional estimation methods and 3D surface fitting. J. Am. Heart Assoc. 8 (6), e009124.

Oktay, O., Ferrante, E., Kamnitsas, K., Heinrich, M.P., Bai, W., Caballero, J., Guerrero, R., Cook, S.A., de Marvao, A., Dawes, T., O'Regan, D.P., Kainz, B., Glocker, B., Rueckert, D., 2017. Anatomically constrained neural networks (ACNN): application to cardiac image enhancement and segmentation. CoRR. abs/1705.08302. arXiv:1705.08302. URL http://arxiv.org/abs/1705.08302.

Osman, A.A., Abumanga, Z.M., 2019. The relationship between physical activity status and dietary habits with the risk of cardiovascular diseases. E J. Cardiovasc. Med. 7 (2), 72.

Pain, C.D., Egan, G.F., Chen, Z., 2022. Deep learning-based image reconstruction and post-processing methods in positron emission tomography for low-dose imaging and resolution enhancement. Eur. J. Nucl. Med. Mol. Imaging 1–21.

Painchaud, N., Skandarani, Y., Judge, T., Bernard, O., Lalande, A., Jodoin, P.-M., 2020. Cardiac segmentation with strong anatomical guarantees. IEEE Trans. Med. Imaging 39 (11), 3703–3713. http://dx.doi.org/10.1109/TMI.2020.3003240.

Palit, A., Bhudia, S., Arvanitis, T., Turley, G., Williams, M., 2018. In vivo estimation of passive biomechanical properties of human myocardium. Med. Biol. Eng. Comput. 56, 1–17. http://dx.doi.org/10.1007/s11517-017-1768-x.

Peirlinck, M., Costabal, F.S., Yao, J., Guccione, J., Tripathy, S., Wang, Y., Ozturk, D., Segars, P., Morrison, T., Levine, S., Kuhl, E., 2021. Precision medicine in human heart modeling. Biomech. Model. Mechanobiol. 20, 803–831.

Rabbani, A., Babaei, M., 2022. Resolution enhancement of placenta histological images using deep learning. In: Proceedings of the 4 Th International Conference on Statistics: Theory and Applications. 155–1–155–5.

Rabbani, A., Babaei, M., Gharib, M., 2022a. Automated segmentation and morphological characterization of placental histology images based on a single labeled image. arXiv preprint arXiv:2210.03566.

Rabbani, A., Gao, H., Husmeier, D., 2022b. Temporal extrapolation of heart wall segmentation in cardiac magnetic resonance images via pixel tracking. In: Proceedings of the 4 Th International Conference on Statistics: Theory and Applications. 154–1–154–5.

Romaszko, L., Borowska, A., Lazarus, A., Dalton, D., Berry, C., Luo, X., Husmeier, D., Gao, H., 2021. Neural network-based left ventricle geometry prediction from CMR images with application in biomechanics. Artif. Intell. Med. 119, 102140.

Romaszko, L., Lazarus, A., Gao, H., Borowska, A., Luo, X., Husmeier, D., 2019. Massive dimensionality reduction for the left ventricular mesh. In: Proceedings of the International Conference on Statistics: Theory and Applications (ICSTA), vol. 1. International ASET.

Ronneberger, O., Fischer, P., Brox, T., 2015. U-net: Convolutional networks for biomedical image segmentation. In: International Conference on Medical Image Computing and Computer-Assisted Intervention. Springer, pp. 234–241.

Rose, S., McGuire, T.G., 2019. Limitations of p-values and R-squared for stepwise regression building: a fairness demonstration in health policy risk adjustment. Amer. Statist. 73 (sup1), 152–156.

Roth, G.A., Mensah, G.A., Johnson, C.O., Addolorato, G., Ammirati, E., Baddour, L.M., Barengo, N.C., Beaton, A.Z., Benjamin, E.J., Benziger, C.P., et al., 2020. Global burden of cardiovascular diseases and risk factors, 1990–2019: update from the GBD 2019 study. J. Am. Coll. Cardiol. 76 (25), 2982–3021.

Stevens, W., Peneva, D., Li, J.Z., Liu, L.Z., Liu, G., Gao, R., Lakdawalla, D.N., 2016. Estimating the future burden of cardiovascular disease and the value of lipid and blood pressure control therapies in China. BMC Health Serv. Res. 16 (1), 1–10.

Voorhees, A., Han, H.-C., 2015. Biomechanics of cardiac function. Compr. Physiol. 5 4, 1623–1644.

Wang, H.M., Gao, H., Luo, X.Y., Berry, C., Griffith, B.E., Ogden, R.W., Wang, T.J., 2013. Structure-based finite strain modelling of the human left ventricle in diastole. Int. J. Numer. Methods Biomed. Eng. 29 (1), 83–103. http://dx.doi.org/10.1002/cnm.2497.

Westermann, D., Kasner, M., Steendijk, P., Spillmann, F., Riad, A., Weitmann, K., Hoffmann, W., Poller, W., Pauschinger, M., Schultheiss, H.-P., Tschöpe, C., 2008. Role of left ventricular stiffness in heart failure with normal ejection fraction. Circulation 117 (16), 2051–2060. http://dx.doi.org/10.1161/CIRCULATIONAHA.107.716886, arXiv:https://www.ahajournals.org/doi/pdf/10.1161/CIRCULATIONAHA.107.716886. URL https://www.ahajournals.org/doi/abs/10.1161/CIRCULATIONAHA.107.716886.

Williams, C.K., Rasmussen, C.E., 2006. Gaussian Processes for Machine Learning, vol. 2/3. MIT press Cambridge, MA.

Wolterink, J.M., Leiner, T., Viergever, M.A., Isgum, I., 2017. Automatic segmentation and disease classification using cardiac cine MR images. CoRR abs/1708.01141. arXiv:1708.01141. URL http://arxiv.org/abs/1708.01141.

Xia, X., Kulis, B., 2017. W-net: A deep model for fully unsupervised image segmentation. arXiv preprint arXiv:1711.08506.

Yan, W., Wang, Y., van der Geest, R.J., Tao, Q., 2019. Cine MRI analysis by deep learning of optical flow: Adding the temporal dimension. Comput. Biol. Med. 111, 103356.

Zhou, Z., Rahman Siddiquee, M.M., Tajbakhsh, N., Liang, J., 2018. Unet++: A nested u-net architecture for medical image segmentation. In: Deep Learning in Medical Image Analysis and Multimodal Learning for Clinical Decision Support. Springer, pp. 3–11.

Zile, M.R., Baicu, C.F., Gaasch, W.H., 2004. Diastolic heart failure—abnormalities in active relaxation and passive stiffness of the left ventricle. N. Engl. J. Med. 350 (19), 1953–1959.